Supplementary Material

Diacetylene Covalent Organic Framework through One-step Two-electron O_2 Reduction Pathway Efficient Photosynthesis H_2O_2

Pengken Li[a], Hui Zhao[a], Rong Ji[a], Wenwen Chi[a], Xinyu Sun[a], Yuming Dong*[a], Yongfa Zhu[b] [a]

[a]   P.K. Li, H. Zhao, R. Ji, W.W. Chi, X.Y. Sun, Y.M. Dong

         International Joint Research Center for Photo-responsive Molecules and Materials, School of Chemical and Material Engineering

         Jiangnan University

         Wuxi 214122 (China)

         E-mail: dongym@jiangnan.edu.cn

[b]   Y.F. Zhu

         Department of Chemistry

         Tsinghua University

         Beijing 100084 (China)

Part 1. Experimental Section

Measurement of hydrogen peroxide. $0.018 mol·L^{-1}$ calibration solution of titanium potassium oxalate containing 5 vol% concentrated sulfuric acid was prepared, and standard curves were made[1]. 1.5 mL of the filtered reaction solution was added to 1 mL of the calibration solution of titanium potassium oxalate. After shaking, the reaction solution was allowed to react thoroughly with titanium potassium oxalate for 10 min. The absorbance (Abs) was measured by UV-vis spectrophotometer at the wavelength of 400 nm, and the H_2O_2 concentration was calculated by comparing the standard curve relation y $(mmol·L^{-1})$ = 1.83986*x (Abs).
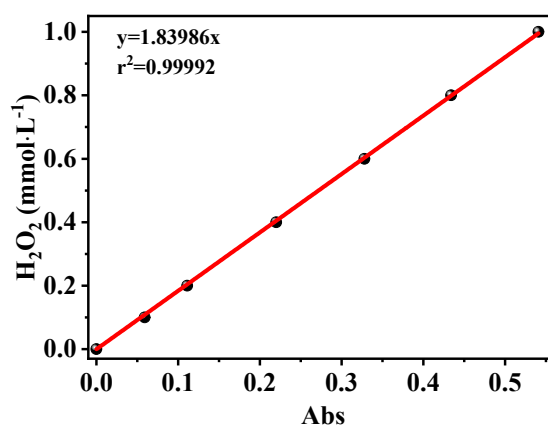

Figure S1. Standard curve of H_2O_2 concentration.

Electrochemical test. The Mottschottky curve and electrochemical impedance (EIS) of the photocatalyst were measured using an electrochemical workstation (CHI 660E), and the transient photocurrent was measured under a 300 W xenon lamp. The electrode system consisted of a working electrode, aluminum foil (26 mm*13 mm* 0.1mm) as a counter electrode, and Ag/AgCl electrode as a reference electrode. FTO coated with a fixed amount of photocatalyst, an area of $1 cm^2$ was used as the working electrode, and 0.5 M Na_2SO_4 was used as the electrolyte.

ITC test. Binding thermodynamics of O_2 to COFs was performed at 25 °C on a titration microcalorimeter (VP-ITC)[2, 3]. The deionized water containing COFs and pure water were loaded in sample and reference cells of the calorimeter, respectively. Degassed saturated oxygen deionized water was sequentially injected (10 uL in eachinjection) into the sample cell containing deionized water containing COFs. The rotating speed of injector was set at 502 rpm. The time duration of each injectionwas 20 s, and delay time between next injections was 180 s.

NBT test. The photocatalytic generation of $·O_2^-$ was determined by the degradation of NBT, which was monitored by the absorbance change at the wavelength of 259 nm. The mole ratio of generated $·O_2^-$ and degraded NBT was 4:1 according to the following equation[4] (eq S1).

$$NBT + 2·O_2^- + 2H^+ = Formazan + 4O_2 \quad (Eq\ S1)$$

UV-Vis DRS spectra and band position calculations. Tauc plots was calculated by the formula:

$$\alpha h\upsilon = A(h\upsilon - E_g)^{\frac{n}{2}} \quad \ldots\ldots\ldots\ldots\ldots \quad \text{Eq. (A.2)}$$

where α, h, ν, Eg and A are the absorption coefficient, Planck's constant, light frequency, band gap energy and a constant, respectively. The n values of CN are 1, which is determined by the optical transition properties of a semiconductor (n = 1 for direct transition and n = 4 for indirect transition).

The band edge positions of the catalysts can be calculated using the following equation:

$$E_{CB} \text{ (V vs. NHE)} = E_{fb} \text{ (V vs. Ag/AgCl)} + 0.22 - X \quad \ldots\ldots\text{Eq. (A.3)}$$

$$E_{VB} = E_{CB} + E_g \quad \ldots\ldots\ldots\ldots\ldots\ldots\ldots\ldots\ldots\ldots\ldots\ldots\ldots\ldots\text{Eq. (A.4)}$$

Where E_{VB} and E_{CB} stand for the valence band edge potential and conduction band edge potential, respectively; $E_{Ag/AgCl}$=0.22V vs. NHE; X is the voltage difference between the conduction band value and the flat potential value, generally 0.1-0.2eV (the conduction bands of n-type semiconductors are normally 0.1-0.2 eV deeper than the flat-band potential), which is set as 0.2 eV in this work.

Rotating Disk Electrode (RRDE) Measurements. The rotating disk electrode (RRDE) was tested in O_2 saturated phosphate buffer solution (0.1 M, pH=6.9), with glassy carbon electrode as the working electrode, Pt ring as the counter electrode and Ag/AgCl electrode as the reference electrode. The potential of the Ag/AgCl reference electrode was converted to the potential of RHE according to the Nernst equation: E (vs.RHE) = E (vs. Ag/AgCl) + 0.0591 × pH + 0.197. The ring potential of the disk electrode was maintained at 1.45 V (vs RHE). The linear sweep voltammetry (LSV) tests were performed at the scan speed of 5 mV/s and revolutions of 900, 1600, and 2500 rpm in an O_2-saturated electrolyte. The number of the transferred electrons was calculated following

$$Eq.(1): n = 4\frac{I_d}{I_d + I_r/N}$$

The selectivity of H_2O_2 was determined by

$$Eq.(2): H_2O_2\% = 200\frac{I_r/N}{I_d + I_r/N}$$

where Id is the disc current and Ir is the ring current. The collection efficiency (N) was

determined to be 37%.

In-situ DRIFTs Characterization. In-situ Fourier transform infrared (in-situ FT-IR) spectroscopy measurements were performed using on a Nicolet iS50 spectrometer (Thermo, USA) using the KBr pellet technique. Fourier-transform spectrometer equipped with a Harrick diffuse reflectance accessory at the Infrared Spectroscopy. Each spectrum was recorded by averaging 64 scans at 8 cm^{-1} spectral resolution. The chamber was sealed with two ZnSe windows. First, the silicon crystal is polished. Briefly, an appropriate amount of 0.5 μm alumina polishing powder is poured onto the polishing machine, and an appropriate amount of ultrapure water is added to make it evenly distributed, and rough polishing is performed at a rotational speed of about 300 or 500. Then, the above process was repeated and the polishing table was thoroughly cleaned before being polished with 0.05 μm silicon oxide polishing powder to achieve a smooth finish. The polished silicon crystals were put into a 50 mL beaker and sequentially sonicated with ultrapure water and ethanol for 5 min and rinsed with ultrapure water to obtain the polished silicon crystals. Next, sample solutions were prepared. 5.0 mg of catalyst was sonicated and dispersed in a mixture of 225 μL of ethanol and 25 μL of Nafion®perfluorinated resin solution. The silicon crystals and the reaction cell were assembled together and then 30 μL of the resulting suspension was uniformly added dropwise to the silicon crystals and dried under an infrared lamp. Finally, we added an appropriate amount of water solution to the reaction cell and connected it to the IR instrument. We tested the instrument by passing O_2 through it and accessing the light source.

DFT Calculations. Geometric optimization was performed using Gauss 09W based on the B3LYP exchange-correlation generalized function, 6-311G(d) basis group, and H_2O as a solvent model, and frequency calculations were also performed to ensure that there are no imaginary frequencies in the stable group state[5-10]. The materials' electrostatic potential distribution and homo and lumo charge distributions were calculated by Gauss View 6.0.

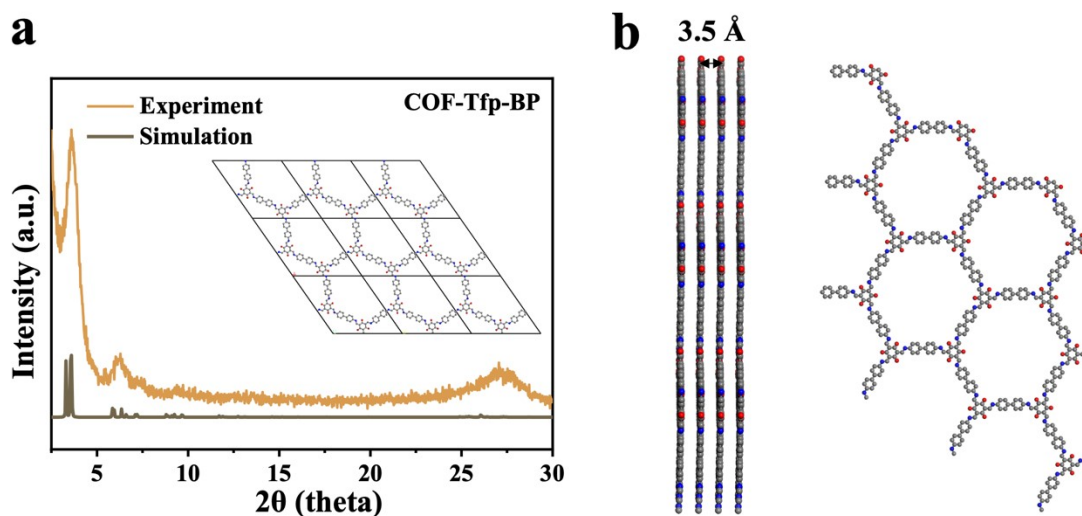# Part2. Additional characterization and experimental data

Figure S2. (a) PXRD patterns: the experimental data and simulated patterns for eclipsed AA stacking mode of COF-Tfp-BP; (b) the modeled crystal structures of COF-Tfp-BP.
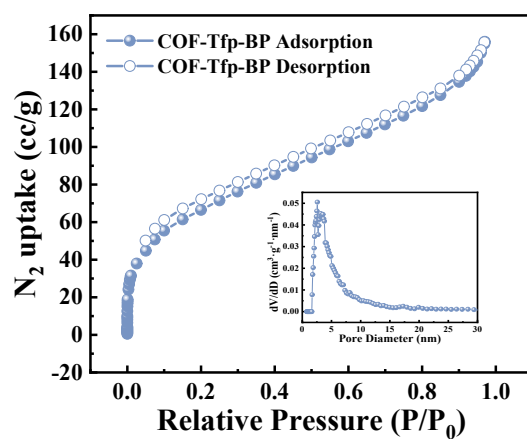

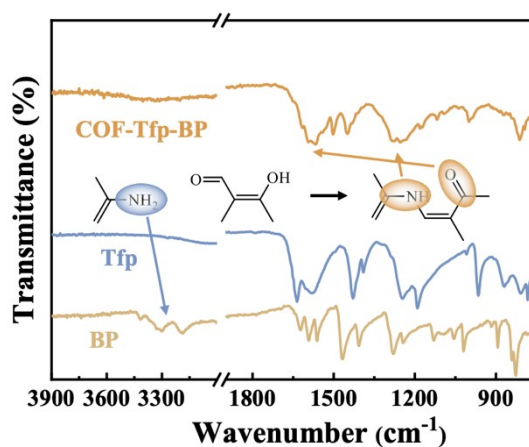Figure S3. N_2 sorption isotherms for COF-Tfp-BP.

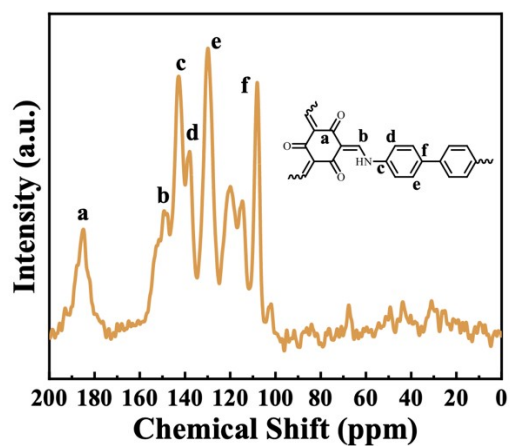Figure S4. FT-IR spectra of COF-Tfp-BP.

Figure S5. NMR spectra of COF-Tfp-BP.

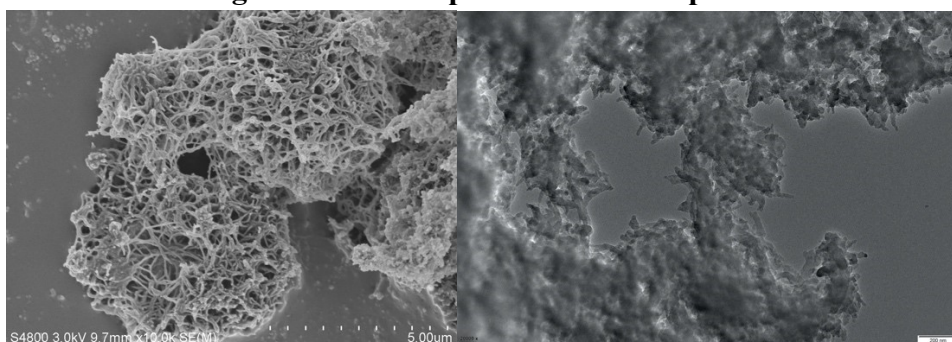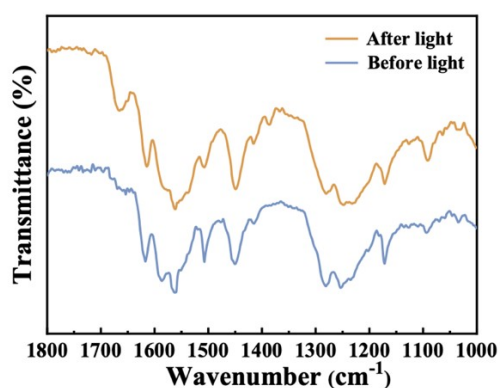**Figure S6. SEM and TEM figure of COF-Tfp-BDDA.**

Figure S7. Comparison of FT-IR spectras before and after COF-Tfp-BDDA reaction.
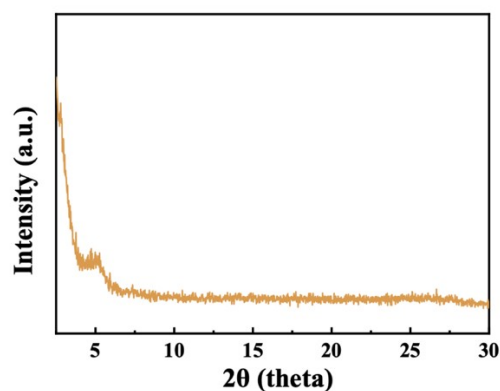
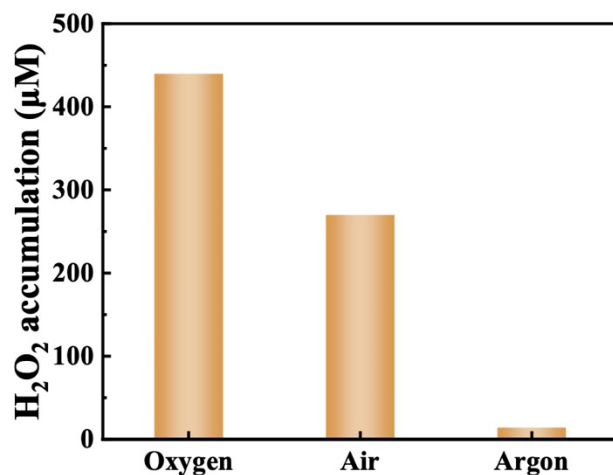**Figure S8. Comparison of PXRD patterns after COF-Tfp-BDDA reaction.**

Figure S9. The H$_2$O$_2$ production of COF-Tfp-BDDA under different conditions (O$_2$, Air, Ar)
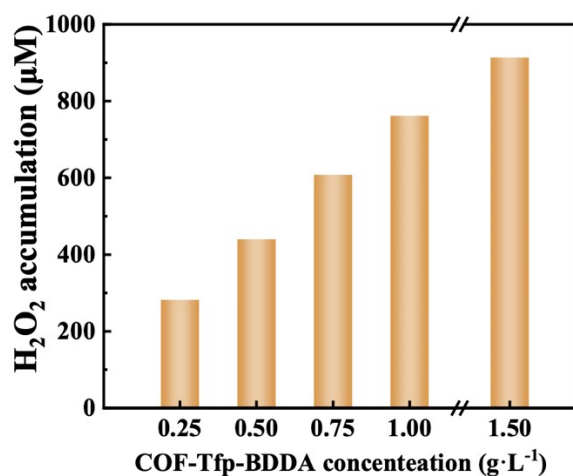

Figure S10. H$_2$O$_2$ production with different amounts of COF-Tfp-BDDA.
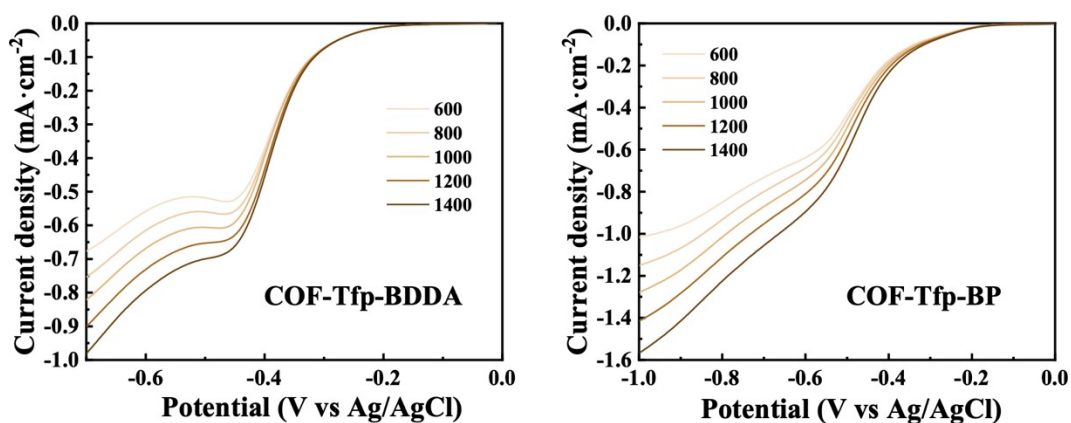

Figure S11. The LSV curves were measured on RRDE with different rotating of COF-Tfp-BDDA and COF-Tfp-BP.
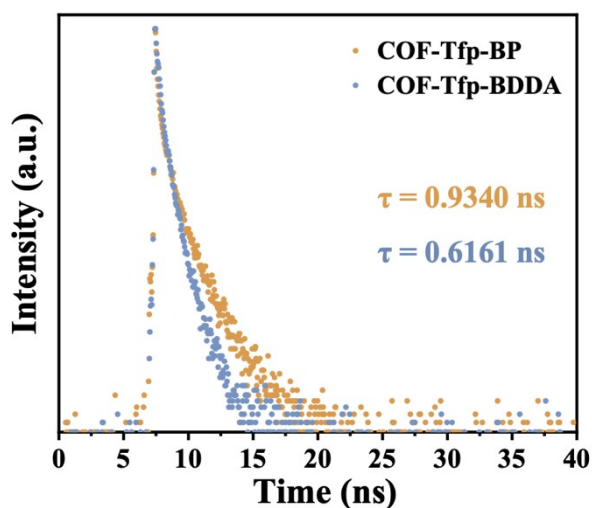
Figure S12. Time-resolved PL decay curves of COF-Tfp-BDDA and COF-Tfp-BP.
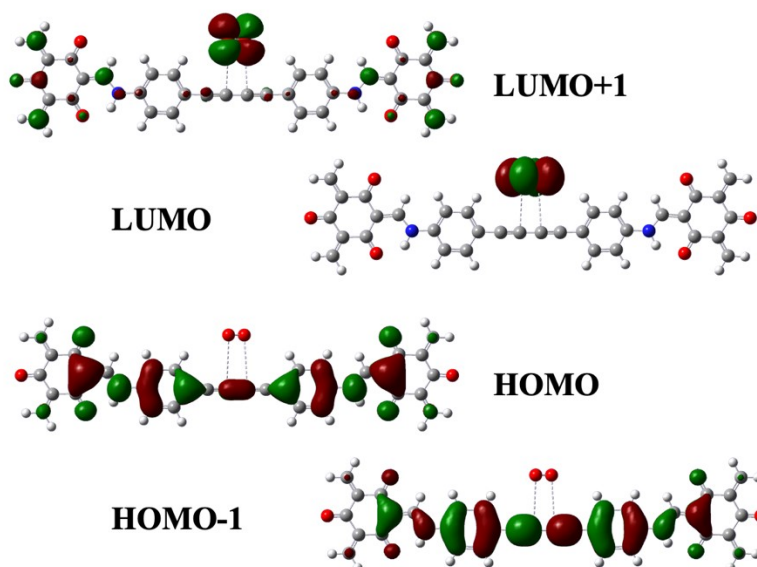

Figure S13. Distributions of the highest occupied molecular orbital (HOMO) and the lowest unoccupied molecular orbital (LUMO), along with those of HOMO-1, HOMO and LUMO, LUMO+1 for the model system of the COF-Tfp-BDDA.
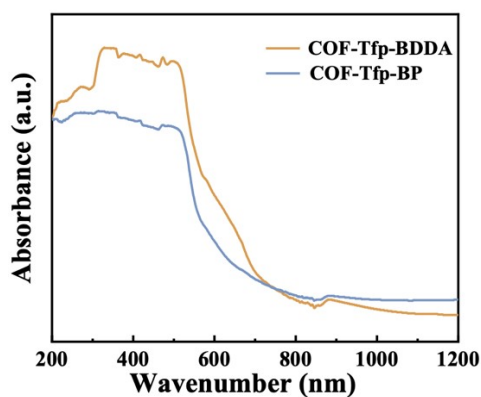

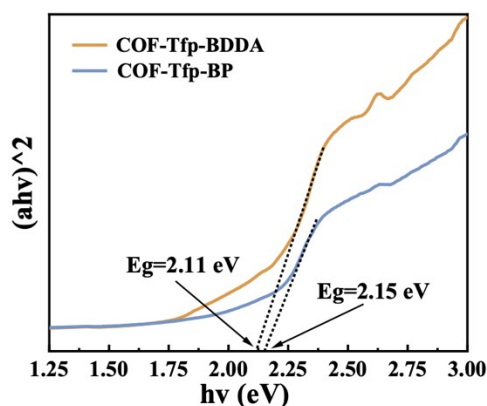**Figure S14. UV- DRS of the resultant COF-Tfp-BDDA and COF-Tfp-BP.**

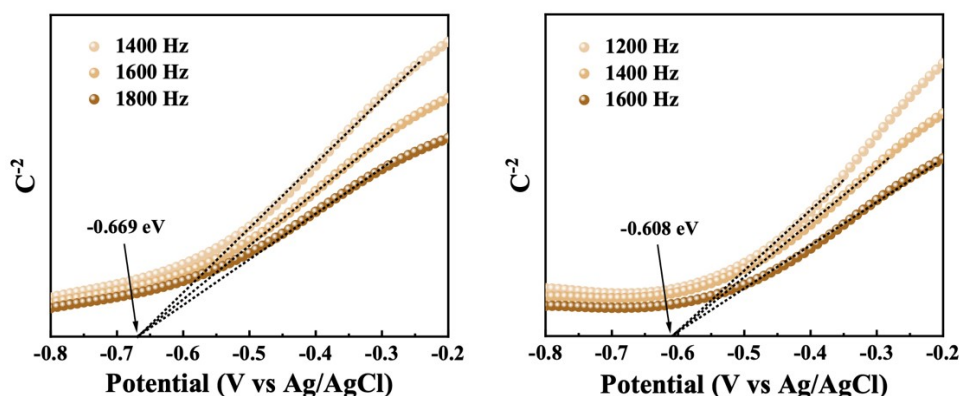**Figure S15. Kubelka-Munk plots of COF-Tfp-BDDA and COF-Tfp-BP.**

Figure S16. Mott−Schottky plot of the COF-Tfp-BDDA and COF-Tfp-BP.
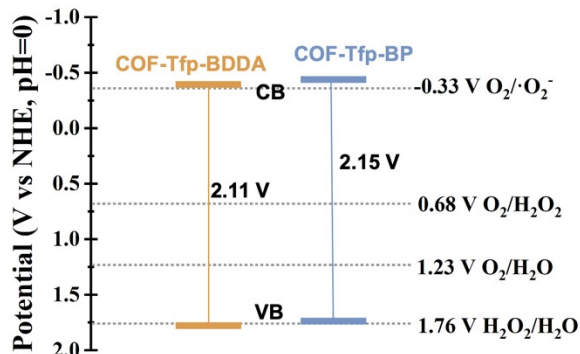

Figure S17. Band alignment of the COF-Tfp-EB and COF-Tfp-PPD.

As the concentration of COF-Tfp-BDDA photocatalyst increased, higher rates of photosynthesized hydrogen peroxide were achieved (Figure S10). However, the rate of photosynthesized hydrogen peroxide did not increase proportionally with the increase of catalyst concentration. This could be attributed to the fact that the increase in suspension concentration caused higher light scattering, resulting in reduced light penetration in the photocatalyst suspension.

The UV-vis near-infrared diffuse reflectance absorption spectra of the two framework materials illustrate significant absorption peaks in the visible range, as depicted in Figure S14. Furthermore, COF-Tfp-BDDA indicates a stronger light absorption range.   Tauc plots and electrochemical Mott-Schottky plots were utilised to ascertain the electronic structure of the fabricated COFs (Figure S16). The bandgap

of COF-Tfp-EB is narrower than that of COF-Tfp-PPD.　　The band gap energy was estimated based on the Tauc plot (Figure S15), where $(\alpha h\upsilon)1/2$ is plotted with respect to the photon energy (where α is the absorption coefficient, h is Planck's constant, and υ is the optical frequency).　　The band gaps obtained for COF-Tfp-BDDA and COF-Tfp-BP were 2.11 eV and 2.15 eV.　　The electrochemical Mott-Schottky plots of the two COFs show positive slopes indicating their n-type semiconducting properties, as shown in Figure S16. The conduction band potentials of COF-Tfp-BDDA and COF-Tfp-BP were -0.669 V (with respect to Ag/AgCl) and -0.608 V (with respect to Ag/AgCl).　　Accordingly, the corresponding conduction band (CB) and valence band (VB) were calculated as shown in Figure S17.　　Both COFs conduction band potentials lie above the potential of the two-electron oxygen reduction pathway, ensuring sufficient reduction potential for H_2O_2 generation.

Reference

1.　　L. Jian, Y. Dong, H. Zhao, C. Pan, G. Wang and Y. Zhu, *Applied Catalysis B: Environmental*, 2024, **342**, 123340.
2.　　C. Hoffmann, A. Blume, I. Miller and P. Garidel, *Eur Biophys J*, 2009, **38**, 557-568.
3.　　H. Wang, T. Li, H. Xiang, X. Zhang, K. Fang, G. Wu, M. Yan, N. Xue, M. Chen, T. Xie, Y. Zhang, P. Wang and H. Lei, *Molecules*, 2017, **22**.
4.　　M. Chen, K. Hagedorn, H. Colfen and S. Polarz, *Adv Mater*, 2017, **29**.
5.　　R. Ditchfield, W. J. Hehre and J. A. Pople, *The Journal of Chemical Physics*, 2003, **54**, 724-728.
6.　　S. Grimme, J. Antony, S. Ehrlich and H. Krieg, *The Journal of Chemical Physics*, 2010, **132**.
7.　　S. Grimme, S. Ehrlich and L. Goerigk, *Journal of Computational Chemistry*, 2011, **32**, 1456-1465.
8.　　A. V. Marenich, C. J. Cramer and D. G. Truhlar, *The Journal of Physical Chemistry B*, 2009, **113**, 6378-6396.
9.　　F. Weigend, *Physical Chemistry Chemical Physics*, 2006, **8**, 1057-1065.
10.　　F. Weigend and R. Ahlrichs, *Physical Chemistry Chemical Physics*, 2005, **7**, 3297-3305.